PHYSICAL REVIEW RESEARCH **6**, L022037 (2024)

Letter | Editors' Suggestion

Single file motion of robot swarms

Laciel Alonso-Llanes, Angel Garcimartín,* and Iker Zuriguel

Depto. de Física y Mat. Apl., Facultad de Ciencias, Universidad de Navarra, E-31080 Pamplona, Spain

(Received 27 February 2024; accepted 22 April 2024; published 10 May 2024)

We present experimental results on the single file motion of a group of robots interacting with each other through position sensors. We successfully replicate the fundamental diagram typical of these systems, with a transition from free flow to congested traffic as the density of the system increases. In the latter scenario we also observe the characteristic stop-and-go waves. The unique advantages of this novel system, such as experimental stability and repeatability, allow for extended experimental runs, facilitating a comprehensive statistical analysis of the global dynamics. Above a certain density, we observe a divergence of the average jam duration and the average number of robots involved in it. This discovery enables us to precisely identify another transition: from congested intermittent flow (for intermediate densities) to a totally congested scenario for high densities. Beyond this finding, the present work demonstrates the suitability of robot swarms to model complex behaviors in many particle systems.

DOI: 10.1103/PhysRevResearch.6.L022037

In recent years, swarm robotics has emerged as a fascinating field where the goal is the design and control of robot ensembles operating as a coordinated system [1–4]. These robots are typically simple and small, and they interact with each other and their environment to achieve a common goal. Despite their limited individual capabilities, they can be programed to collaboratively perform complex tasks such as searching for objects, exploring unknown environments, or transporting objects. Robot swarms also provide a unique platform for studying collective behavior. For instance, kilobots [5–7], characterized by their compact size, straightforward design, and controllability through an open-source platform, stand out as excellent agents for conducting large-scale studies involving hundreds of units. Importantly, two distinct approaches can be adopted in the investigations of collective motion with robot swarms: (i) a pragmatic approach primarily focused on the task to be performed, where the robot rules are fine-tuned to optimize the collective performance; and (ii) a bottom-top approach in which the motion and interaction rules among the agents are established and the emerging macroscopic dynamics are analyzed. We took the latter one, which resembles the traditional approach implemented in the science of complex systems such as active matter, pedestrian crowd dynamics, and collective animal behavior.

We have used an assembly of palm-sized robots that incorporate an on-board nanocomputer, which allows a high degree of control and flexibility on the programed interactions—significantly greater than the simpler kilobots, for instance. The trade off is a reduction in the number of agents that make up the swarm, with a hundred being a reasonable upper limit. Weighing the advantages against the disadvantages, we propose this robot swarm as a suitable framework to investigate the emergence of collective behaviors in active matter such as self-organization in confined geometries [8], clogging in bottleneck flows [9], segregation driven by counterflow [10], and any other scenario where the role of inertia or physical contacts between agents is significant.

As a starting point, we have chosen investigating the motion in a single file experiment. The main reason for this choice lies in the simplicity of the system, but also the extensive number of experiments developed on this topic [11], especially in fields such as vehicular traffic [12,13] and pedestrian dynamics [14–16], but also for active systems in general [17–19]. Additionally, there exists a theoretical framework [20–23] against which we can contrast our findings. Essentially, the main features observed in single file motion include (i) a transition from free flow to a congested flow as density (number of agents per unit length) increases; and (ii) the spontaneous emergence of stop-and-go waves traveling backwards. Also, the single file geometry has been largely used to investigate the dependence of the flow rate on the density in pedestrian dynamics, a representation known as the fundamental diagram [24–26]. Perhaps the main drawback of the experiments conducted thus far is the limitation in the duration of the experimental runs, along with a lack of control and stability over the experimental conditions. We remark that pedestrian dynamics and vehicular traffic are affected by human behavior changing over time, due to factors such as tiredness or boredom. In other active systems, maintaining experimental conditions unaltered can also be a challenging task. It is precisely on this point that experiments with robots can be extremely useful, since their behavior remains constant over time with the only limitation being the duration of the batteries (more than one hour in our case). Therefore, this

*angel@unav.es

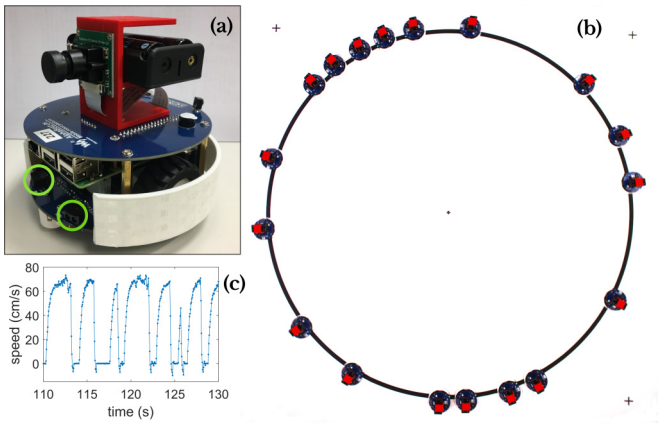

FIG. 1. (a) Photograph of a robot. Green circles mark the infrared proximity sensors. (b) Snapshot of 18 robots on the circular lane; a jam of five robots can be seen at approximately 11 o'clock. (c) Single-robot speed over a 20-second interval in an experiment with $N = 20$ robots and $V_{\max} = 69$ cm/s. The short peaks of negative velocity are due to the robot swinging forth and back when coming to a stop.

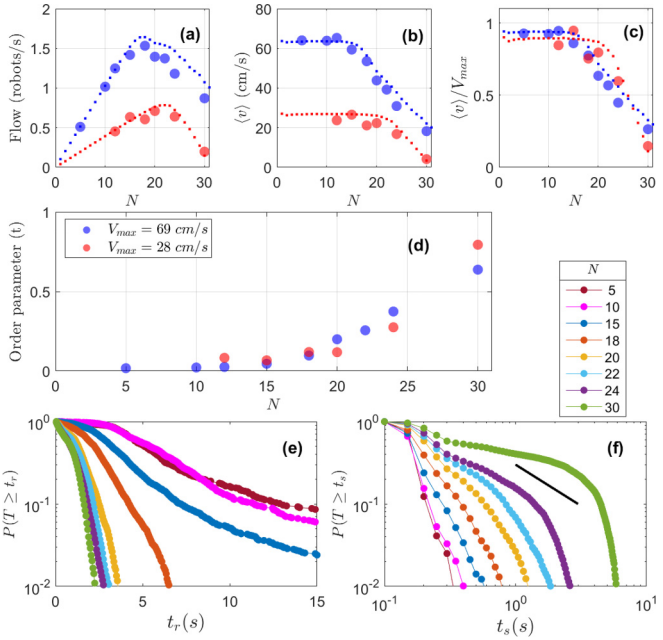

FIG. 2. (a) Average flow rate versus the number of robots in the system (N) for two different robot speeds [$V_{\max} = 28$ cm/s and $V_{\max} = 69$ cm/s, as indicated in the legend of (d)]. Solid lines are results of numerical simulations. (b) Average speed $\langle v \rangle$ as a function of the number of robots N. (c) Rescaled speed (i.e., the average speed divided by robot speed $V_{\max}$), as a function of N. (d) Order parameter t as a function of N. (e) Log-lin survival function of the time lapse that an individual robot is running t_r, for scenarios with $V_{\max} = 69$ cm/s and different N [as indicated in the legend above panel (f)]. (f) Survival function of the time lapse that an individual robot is stopped t_s in log-log scale. The solid line has a slope of -1, hence corresponding to a power-law exponent of -2.

system enables the implementation of long and steady experimental runs, a critical factor in revealing certain distinctive statistical features of the collective dynamics.

Our robots are 11 cm in diameter [Fig. 1(a)] and are constructed using the Alphabot2 platform, a kit manufactured by Waveshare, which incorporates a Raspberry Pi nanocomputer. They are driven by two wheels propelled by DC motors and are equipped with various elements enabling control over interactions with other agents and the environment. Infrared (IR) sensors at the base can detect a dark line and follow it by regulating the power delivered to each wheel; a PID loop is used to this end. Two infrared sensors at the front detect obstacles or other robots within a tunable distance; for this work, we have set the maximum distance to 15 cm [27]. We remark that in the experimental conditions (curvature, irregular line following, and so on) the average detection distance displays important variations, resulting in an average of 11 ± 3 cm (the error is given as half the interquartile range). The robot speed can be adjusted by changing the motor duty cycle; here we tested speeds ranging from about 20 to 80 cm/s. Remarkably, the speed exhibits slight variations from one robot to another, with an interquartile range of about 10% for a given duty cycle. On top of the standard equipment, our robots have been upgraded by including a red support for the camera (also used for tracking robots), batteries with greater capacity, and a white, reflective shell. The on-board computers are connected to an external computer via WiFi, allowing remote access and operation. For detailed information about the robot features, see the Supplemental Material (SM) [27].

At the beginning of an experimental run, a set of N robots is arranged at equal intervals atop a 2 m diameter circular black line [Fig. 1(b)]. All robots receive the same configuration defining operational parameters, and they are set into motion simultaneously. Subsequently, robots follow the line at the prescribed speed and stop whenever they detect another robot in front of them. Then, as soon as the sensors do not detect anything in front, the robot resumes motion. Therefore, the nominal speed can be zero (robot stopped) or $V_{\max}$ (the "free speed"). Crucially [28,29], the braking is more abrupt than the acceleration, as evidenced in the speed vs time graph of a single robot represented in Fig. 1(c). When $V_{\max} = 69$ cm/s, it takes approximately 0.1 s to reduce $V_{\max}$ by one half, while about 0.3 s are needed to accelerate from zero to $V_{\max}/2$ [27]. The motion of the robots is recorded with a video camera from above with a resolution of 2600×2600 pixels at 20 frames per second (see the video in [27]). We register several runs of three minutes for each set of conditions. From these, we obtain the robot position by analyzing each frame and detecting the center of red squares, hence obtaining a file with the robot number, time, and position, with an accuracy of ± 0.05 s in time and ± 2 mm in position.

We first show the dependence of macroscopic quantities, such as flow and velocity, on the number of robots N in the system. In Fig. 2(a) we observe the existence of a region of free flow where the flow grows linearly with N, and then a congested region where the flow decreases with N. This observation holds for all nominal free velocities, $V_{\max}$, although only two (28 cm/s and 69 cm/s) are shown in the plot. The existence of these two regimes is also apparent in the representation of the average robot velocity ($\langle v \rangle$) versus N. In the free flow region, $\langle v \rangle$ remains constant and does not depend on N, whereas in the congested region it noticeably decreases

with N. The transition seems to occur in the range $15 < N < 18$ irrespective of $V_{\max}$. This characteristic is underscored in Fig. 2(c) when normalizing the average velocity to $V_{\max}$. A standard way to visualize this transition is by computing the fraction of time that the agents are stopped $t = \frac{t_s}{t_s+t_r}$, where t_s and t_r are the times that the robots are stopped and running, respectively. Results [Fig. 2(d)] show that t is close to zero up to $15 < N < 18$ and increases beyond this point, confirming the existence of the transition.

Taking a further step, we investigated the features of the collective motion by examining the statistics of running and stop intervals through survival functions (i.e., the probability of finding an interval lasting longer than a given time). To this end, we focused on the case $V_{\max} = 69\,\mathrm{cm/s}$ (similar outcomes are obtained for other velocities). The running intervals [Fig. 2(e)] exhibit a clear change in trend at $15 < N < 18$; for larger N, the distributions appear to follow an exponential pattern, while the tails broaden for smaller N (free flow region) due to robots experiencing unboundedly long t_r. Similarly, the distributions of t_s [Fig. 2(f)] show an increase in stopped time as N grows. Interestingly, for $N = 30$ the distribution seems compatible with a power law with an exponent smaller than two (indicated by the black line as a reference), at least for a small range of $0.3 < t_s < 3$ seconds. If confirmed, this observation will have significant consequences, as a power-law distribution with an exponent smaller than two implies a lack of convergence of its first moment (i.e., the average) [30]. This suggests the possible existence of another transition (for systems with very high densities) to a region with different behavior, where the time a robot remains stopped diverges. Unfortunately, we cannot verify if this power-law tail extends over a broader range of t_s values, as there is an intrinsic temporal cutoff determined by the system size and number of robots: a robot cannot be stopped longer than the time it takes for all robots in front of it to start moving. In other words, despite the analysis of stopping times hinting at the existence of a transition to a fully congested state when $N \approx 30$, this parameter does not appear to be the most suitable for drawing a definitive conclusion.

Motivated by this discovery, we focused on jam formation and the characteristics of stop-and-go waves, typical of these systems. In Figs. 3(a)–3(c), we present a portion of the spatiotemporal diagrams constructed with the angular position of each robot (x axis) versus time (increasing downwards on the y axis). When $N = 10$ [Fig. 3(a)], the robots (each represented by a line) move toward the right (increasing values of angle) with short jams appearing only occasionally (red segments). As N increases [Fig. 3(b)], jams become more frequent, and they clearly propagate backwards (from right to left as time increases). Finally, for $N = 30$ [Fig. 3(c)], jams increase in size (number of robots involved) and live longer. The jammed regions (red segments) seem to percolate under these conditions. From this visual representation, we proceeded to obtain the survival functions of jam lengths (l, denoting the number of robots involved in the jam) for different values of N [Fig. 3(d)]. Note that these plots are only meaningful when jams involving more than a few robots are formed (i.e., for $N \geqslant 15$). Interestingly, we observe that the distributions for $N = 24$ and $N = 30$ are compatible with power law decays with an exponent smaller than two. As mentioned earlier, this

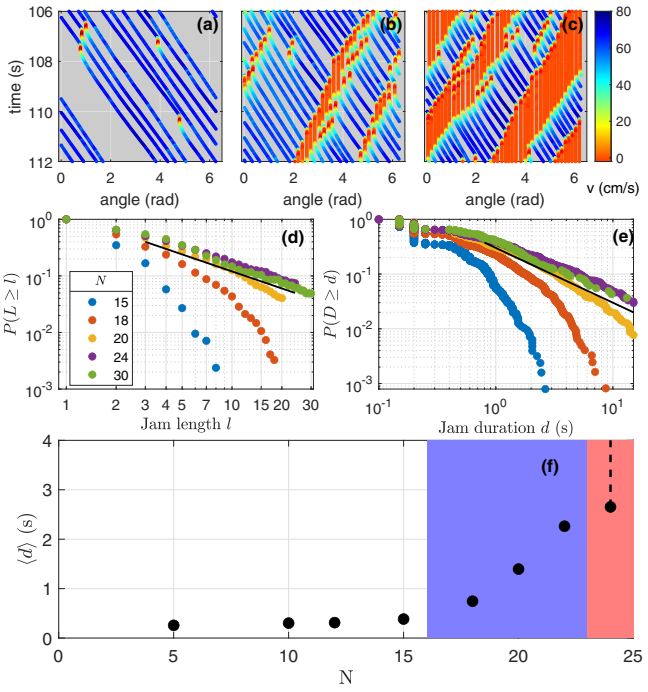

FIG. 3. (a)–(c) Spatiotemporal diagrams depicting six seconds of experimental results with $V_{\max} = 69\,\mathrm{cm/s}$ and $N = 10$, 20, and 30 robots, respectively. Speeds are color coded as shown in the color bar. (d) Survival function of the jam length (l) for $V_{\max} = 69\,\mathrm{cm/s}$ and different numbers of robots (N), as indicated in the legend. Note the logarithmic scale. (e) Survival function in logarithmic scale for the jam duration d. Solid lines serve as guides to the eye, illustrating an exponent of -1 which power law tails with an exponent of -2 in the probability density. (f) Average jam duration $\langle d \rangle$ as a function of N. The point corresponding to $N = 24$ represents the average of the registered data; we remark, however, that this value does not accurately reflect convergence of the first moment, as $\langle d \rangle$ grows unboundedly with the measuring time. This is indicated with the dashed line.

implies that average jam lengths grow unboundedly with the measuring time window, suggesting a state of total congestion. But once again we face the problem of distributions spanning less than one order of magnitude (at most, from $l = 3$ to $l = 30$). This limitation is, of course, imposed by the number of robots in the ensemble.

A way to overcome this restriction is to examine the statistics of jam duration, a variable constrained only by the length of the experimental runs. Once again, the survival distributions of jam durations [Fig. 3(e)] are compatible with power-law decays with exponents smaller than two in absolute value for $N = 24$ and $N = 30$. In this case, the power laws span over almost two orders of magnitude over the time axis. From this observation, we can represent the average duration of jams $\langle d \rangle$ vs N, obtaining three well differentiated regions [Fig. 3(f)]. For diluted systems ($N < 15$) jams are sporadic, last for very short periods of time, and are typically caused by just one robot moving a little bit more slowly than the one behind it; therefore, $\langle d \rangle \approx 0$. As N increases jams begin to appear in earnest, leading to finite values of $\langle d \rangle$. Importantly, jam persistence gives rise to the characteristic emergence of

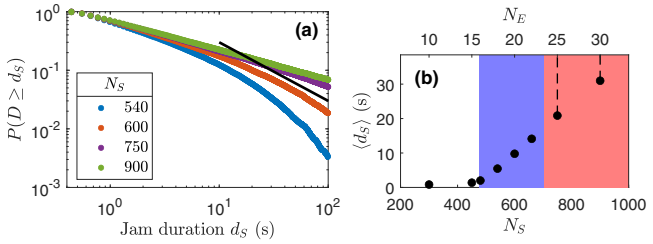

FIG. 4. (a) Survival function for jam duration in simulations (d_S) for different number of agents (N_S). The solid line serves as a guide to the eye, illustrating an exponent of -1 in the survival, corresponding to power laws with an exponent of -2. Note the logarithmic scale. (b) Average jam duration $\langle d_S \rangle$ as a function of N_S. The top axis indicates the number of agents (N_E) corresponding to systems with equal density and the size of the experimental scenario.

stop-and-go waves. Finally, for still larger values of N, jam duration diverges, in the sense that the calculation of its average depends on the time window employed (the longer the measurement, the higher the average duration). In Fig. 3(f) this is represented by a dot with a dashed line in the vertical direction, indicating that the average value calculated would tend to infinity for infinitely long measurements. More importantly, this behavior can be associated with a totally congested scenario in which the jam duration and size percolate through the whole system.

From these experimental results, a concern may arise regarding whether the transition to totally congested flow is caused by finite-size effects. To address this issue, we conducted numerical simulations using a variation of the Nagel-Schreckenberg cellular automaton model for freeway traffic [20]. We implemented a one-dimensional array of $L = 333$ sites with periodic boundary conditions where we evenly distribute N_S simulated agents. Agents are initially at rest and start moving, increasing their speed by one unit per simulation step until reaching a maximum speed $V_{S\,\max}$ (different runs were implemented with $V_{S\,\max} = 2$ and 4 sites/step). To introduce some degree of randomness in speed, at each time step each agent has a probability $p = 0.2$ to reduce it by one unit. Moreover, agents stop to avoid collisions with preceding ones; and ghosting overtakes are also forbidden. Each simulation run lasts for 200 steps and ten repetitions are implemented for each set of parameters (see the SM for additional details).

First, we tried to reproduce the behavior of macroscopic quantities reported in Figs. 2(a)–2(c). Importantly, to reach this goal we needed to implement a feature accounting for the detection distance at which the robots stop moving. This was accomplished by defining a detection threshold of $d_d = 9$ cells; when the preceding agent is less than d_d cells away, the simulated agent stops. This introduces randomness in the stopping distance (as it ranges from $d_d = 9$ to $d_d - V_{S\,\max}$), a phenomenon also observed in the experiments. As evidenced by the lines in Figs. 2(a)–2(c), the agreement between simulations and experiments is quite good. Building on this, we extended the system size to 10^4 sites and computed the distributions of jam duration d_S for a different number of simulated agents N_S [Fig. 4(a)]. Remarkably, we qualitatively reproduce the trends observed experimentally, with the transition to a totally congested scenario (exponent below one in the survival function) taking place at about $N_S = 750$. The representation of the average jam duration $\langle d_S \rangle$ vs N_S [Fig. 4(b)] also exhibits a behavior similar to the experimental one, although the transitions occur at higher values of N_S. Interestingly, if we calculate how many robots in the experiment would correspond to the densities simulated with N_S and 10^4 sites [N_E, see top x axis in Fig. 4(b)], we achieve a reasonable agreement with the experimental results. These findings confirm that the existence of three distinct phases (flowing, congested, and totally congested) is an intrinsic hallmark of the studied system that emerges independently of its size.

In conclusion, we report experimental and numerical results of the single file motion of a robot swarm where we reproduce the transition from a free flow phase to a congested one, characterized by intermittent flow and the emergence of stop-and-go waves due to the development of jams. Moreover, the statistical analysis of the jam size and duration enables to discern a transition to a totally congested scenario wherein jams percolate over the entire system, and their average duration diverges. Beyond the interesting features reported, this work showcases the great potential of robotic systems to reproduce complex collective behavior observed in various fields, including active matter and pedestrian dynamics. Among the main advantages of this system, we highlight the temporal stability of the experimental conditions, the high degree of control over various parameters (including speed, force, reaction time, and interparticle distance [31]), and the versatility in terms of the situations that can be implemented thanks to the robot programmable capabilities. A near future challenge involves extending the experiments to bidimensional scenarios and enhancing control over robot-robot communication to account not only for short range, but also for long range interactions.

We specially acknowledge L. F. Urrea for technical help. This work has been funded by the Spanish Government, through Grant No. PID2020-114839GB-I00 supported by MCIN/AEI/10.13039/501100011033.

[1] M. Brambilla, E. Ferrante, M. Birattari, and M. Dorigo, Swarm robotics: a review from the swarm engineering perspective, Swarm Intell. **7**, 1 (2013).

[2] M. Dorigo, G. Theraulaz, and V. Trianni, Swarm robotics: Past, present, and future [Point of view], Proc. IEEE **109**, 1152 (2021).

[3] G. Beni, Swarm intelligence, in *Complex Social and Behavioral Systems*, Encyclopedia of Complexity and Systems Science Series, edited by M. Sotomayor, D. Pérez-Castrillo, and F. Castiglione (Springer, New York, 2020), pp. 791–818.

[4] H. Hamann, *Swarm Robotics: A Formal Approach* (Springer, Cham, Switzerland, 2018).

[5] M. Rubenstein, C. Ahler, and R. Nagpal, Kilobot: A low cost scalable robot system for collective behaviors, in *Proceedings of the 2012 IEEE International Conference on Robotics and Automation* (IEEE Press, Piscataway, NJ, 2012), pp. 3293–3298.

[6] M. Rubenstein, C. Ahler, N. Hoff, A. Cabrera, and R. Nagpal, Kilobot: A low cost robot with scalable operations designed for collective behaviors, Robot. Auton. Syst. **62**, 966-975 (2014).

[7] C. Dimidov, G. Oriolo, and V. Trianni, Random walks in swarm robotics: an experiment with kilobots, in *Proceedings of the International Conference on Swarm Intelligence* (Springer, Cham, Switzerland, 2016), pp. 185–196.

[8] N. A. Araújo, L. M. C. Janssen, T. Barois, G. Boffetta, I. Cohen, A. Corbetta, O. Dauchot, M. Dijkstra, W. M. Durham, A. Dussutour *et al.*, Steering self-organisation through confinement, Soft Matter **19**, 1695 (2023).

[9] G. A. Patterson, P. I. Fierens, F. Sangiuliano Jimka, P. G. König, A. Garcimartín, I. Zuriguel, L. A. Pugnaloni, and D. R. Parisi, Clogging transition of vibration-driven vehicles passing through constrictions, Phys. Rev. Lett. **119**, 248301 (2017).

[10] D. Chowdhury, A. Schadschneider, and K. Nishinari, Physics of transport and traffic phenomena in biology: from molecular motors and cells to organisms, Phys. Life Rev. **2**, 318 (2005).

[11] A. Taloni, O. Flomenbom, R. Castañeda-Priego, and F. Marchesoni, Single file dynamics in soft materials, Soft Matter **13**, 1096 (2017).

[12] Y. Sugiyama, M. Fukui, M. Kikuchi, K. Hasebe, A. Nakayama, K. Nishinari, S. Tadaki, and S. Yukawa, Traffic jams without bottlenecks-experimental evidence for the physical mechanism of the formation of a jam, New J. Phys. **10**, 033001 (2008).

[13] J. Zhang, W. Mehner, S. Holl, M. Boltes, E. Andresen, A. Schadschneider, and A. Seyfried, Universal flow-density relation of single-file bicycle, pedestrian and car motion, Phys. Lett. A **378**, 3274 (2014).

[14] A. Seyfried, B. Steffen, W. Klingsch, and M. Boltes, The fundamental diagram of pedestrian movement revisited, J. Stat. Mech. (2005) P10002.

[15] S. Cao, J. Zhang, D. Salden, J. Ma, and R. Zhang, Pedestrian dynamics in single-file movement of crowd with different age compositions, Phys. Rev. E **94**, 012312 (2016).

[16] T. Lu, Y. Zhao, P. Wu, and P. Zhu, Dynamic analysis of single-file pedestrian movement with maintaining social distancing in times of pandemic, J. Stat. Mech. (2021) 093402.

[17] K. Nishinari, K. Sugawara, T. Kazama, A. Schadschneider, and D. Chowdhury, Modelling of self-driven particles: Foraging ants and pedestrians, Physica A **372**, 132 (2006).

[18] N. J. Suematsu, S. Nakata, A. Awazu, and H. Nishimori, Collective behavior of inanimate boats, Phys. Rev. E **81**, 056210 (2010).

[19] G. A. Patterson and D. R. Parisi, Fundamental diagram of vibration-driven vehicles, arXiv:2311.01211.

[20] K. Nagel and M. Schreckenberg, A cellular automaton model for freeway traffic, J. Phys. I France **2**, 2221 (1992).

[21] S. Krauss, P. Wagner, and C. Gawron, Continuous limit of the Nagel-Schreckenberg model, Phys. Rev. E **54**, 3707 (1996).

[22] A. Schadschneider, The Nagel-Schreckenberg model revisited, Eur. Phys. J. B **10**, 573 (1999).

[23] T. Nagatani, The physics of traffic jams, Rep. Prog. Phys. **65**, 1331 (2002).

[24] L. D. Vanumu, K. Ramachandra Rao, and G. Tiwari, Fundamental diagrams of pedestrian flow characteristics: A review, Eur. Transp. Res. Rev. **9**, 49 (2017).

[25] D. Chowdhury, L. Santen, and A. Schadschneider, Statistical physics of vehicular traffic and some related systems, Phys. Rep. **329**, 199 (2000).

[26] D. R. Parisi, A. G. Sartorio, J. R. Colonnello, A. Garcimartín, L. A. Pugnaloni and I. Zuriguel, Pedestrian dynamics at the running of the bulls evidence an inaccessible region in the fundamental diagram, Proc. Natl. Acad. Sci. USA **118**, e2107827118 (2021).

[27] See Supplemental Material at http://link.aps.org/supplemental/10.1103/PhysRevResearch.6.L022037 for details about robot features, experimental procedures and numerical simulations.

[28] A. Schadschneider and M. Schreckenberg, Traffic flow models with 'slow-to-start' rules, Ann. Phys. **509**, 541 (1997).

[29] K. Nagel and M. Paczuski, Emergent traffic jams, Phys. Rev. E **51**, 2909 (1995).

[30] A. Clauset, C. R. Shalizi, and M. E. J. Newman, Power-law distributions in empirical data, SIAM Rev. **51**, 661 (2009).

[31] R. S. Negi, P. Iyer, and G. Gompper, Controlling inter-particle distances in crowds of motile, cognitive, active particles. arXiv:2402.03851.